MODELING OF ELASTIC WAVE PROPAGATION ON IRREGULAR TRIANGULAR GRIDS USING A FINITE-VOLUME METHOD

Bertram Nolte

Earth Resources Laboratory
Department of Earth, Atmospheric, and Planetary Sciences
Massachusetts Institute of Technology
Cambridge, MA 02139

ABSTRACT

We present a finite-volume method for the modeling of wave propagation on irregular triangular grids. This method is based on an integral formulation of the wave equation via Gauss's theorem and on spatial discretization via Delaunay and Dirichlet tessellations. We derive the equations for both SH and P-SV wave propagation in 2-D. The method is of second-order accuracy in time. For uniform triangular grids it is also second-order accurate in space, while the accuracy is first-order in space for nonuniform grids.

This method has an advantage over finite-difference techniques because irregular interfaces in a model can be represented more accurately. Moreover, it may be computationally more efficient for complex models.

INTRODUCTION

One of the most commonly used modeling approaches for 2-D or 3-D elastic wave propagation is the finite-difference (FD) method (e.g., Virieux, 1984) which traditionally uses uniform rectangular grids. This method has the following drawbacks:

- Irregular interfaces that are present in a model have to be approximated by discrete steps in the grid, which can lead to numerical inaccuracies.
- Surface topography cannot be easily included in the model.
- For a given frequency the number of grid points needed is a function of the wave speed; the higher the wave speed the fewer grid points are needed. However, since

a standard FD approach uses a uniform grid, the grid spacing everywhere in the model is controlled by the region with the lowest wave speed, which often leads to high computation times.

- Similarly, if some part of the model has a detailed structure which requires dense grid spacing, this same spacing must be used throughout the entire model.

In this paper, we develop a method that allows the grid to be irregular and thus does not suffer from any of the above disadvantages. Our method based on solving the wave equation in integral form via the application of Gauss's theorem, the so-called finite-volume (FV) technique. Previously, FV has been applied to elastic wave propagation by Dormy and Tarantola (1995). Our method differs from theirs in the way the grids are defined. It is more similar to the method developed by Lee *et al.* (1994) for the modeling of electromagnetic wave propagation. One advantage of our method over the technique of Dormy and Tarantola (1995) is that boundary conditions can be easily implemented.

Even though we only consider 2-D wave propagation, the method can be easily extended to 3-D.

SH WAVES IN 2-D

First, we consider SH-propagation in 2-D. We assume the waves propagate in the plane $y = 0$; they are thus polarized in the y-direction. The wave equation for this case is

$$\rho \frac{\partial v_y}{\partial t} = \nabla \cdot \sigma \tag{1}$$

where

$$\sigma = [\sigma_{xy}, \sigma_{zy}]^T$$

are the y-components of stress, v_y is the y-component of particle velocity, and ρ is the mass density. The integration of Eq. (1) over an area A with boundary ∂A and the application of Gauss's theorem yields

$$\iint_A dA\, \rho \frac{\partial v_y}{\partial t} = \oint_{\partial A} ds\, \sigma \hat{n}. \tag{2}$$

From Hooke's law we obtain for the time derivatives of the stress components

$$\begin{aligned} \frac{\partial \sigma_{xy}}{\partial t} &= \mu \frac{\partial v_y}{\partial x} \\ \frac{\partial \sigma_{zy}}{\partial t} &= \mu \frac{\partial v_y}{\partial z}, \end{aligned} \tag{3}$$

where μ is the Lamé parameter.

We now define the stress in a local coordinate system $\{\hat{n}, \hat{s}\}$ (Figure 1) in which $\hat{n}$ and $\hat{s}$ are unit vectors that are normal and tangent to the curve ∂A of Eq. (2). In this coordinate system Eq. (2) can be written as

$$\iint_A dA\, \rho \frac{\partial v_y}{\partial t} = \oint_{\partial A} ds\, \sigma_{yn} \tag{4}$$

and analogously to Eq. (3) we obtain for the time derivative of the normal stress component

$$\frac{\partial \sigma_{ny}}{\partial t} = \mu \frac{\partial v_y}{\partial n}. \tag{5}$$

DELAUNAY AND DIRICHLET TESSELLATIONS

For the spatial discretization of equations (4) and (5) we use Delaunay and Dirichlet tessellation (Figure 2). We define these tessellation in the same way as Miller and Wang (1994). Let Ω be a 2-D domain on which the variables in Eqs. (4) and (5) are defined. Let T be a partitioning of Ω by the triangular elements and let $X = \{x_i\}$ denote the set of all vertices of T. Then T is a Delaunay mesh if, for any element of T, the circumcircle (the circle containing the three points of the triangle) of the element contains no other vertices in X (Delaunay, 1934). The Delaunay mesh is represented by solid lines in Figure 2. The Dirichlet tessellation D corresponding to the Delaunay mesh T is defined by $D = \{d_i\}$ where

$$d_i = \{x \in \Omega : |x - x_i| < |x - x_j|, x_j \in X, j \neq i\}$$

for all $x_i \in X$ (Dirichlet, 1850). In other words, d_i describes the region that is closer to the Delaunay vertex x_i than to any other Delaunay vertex. The boundary ∂d_i of d_i is called the Voronoi polygon and is obtained by connecting the circumcenters (the centers of the circumcircles) of the elements of T which have x_i in common. The Voronoi polygons are shown as dashed lines in Figure 2. Also shown is a circumcircle of a Delaunay element which can be seen to have its center at a Voronoi vertex. The Voronoi polygon has the important property that it consists of the perpendicular bisectors of the edges of the Delaunay triangles. We make use of this property in the following section.

DISCRETE EQUATIONS

For the discretization of Eqs. (4) and (5) we use the indexing illustrated in Figure 3. The velocities are updated on the vertices of the Delaunay grid (circles in Figure 3), while stresses are updated at the points where the Voronoi polygon intersects the Delaunay grid, i.e., halfway between the Delaunay vertices (triangles in Figure 3). The material properties ρ and μ are assumed to be constant within each Delaunay element.

Equation (4) is then approximated as

$$\left(\sum_{k=1}^{N_k} A_{[j,k]}\rho_{[j,k]}\right)\frac{v_j^m - v_j^{m-1}}{\Delta t} = \sum_{k=1}^{N_k}\sigma_{[j,k]}^{m-1/2} l_{[j,k]}. \tag{6}$$

Here, N_k is the number of neighbors of point j which is also the number of sides of the Voronoi polygon. $A_{[j,k]}$ is an area element which is defined in Figure 3, v_j^m is the y-component of the particle velocity at point j at the m-th time step, $l_{[j,k]}$ is the length of the line element on the Voronoi polygon between the velocity points k and j, and $\sigma_{[j,k]}$ is the normal stress on this line element.

From Eq. (5) we obtain a discrete approximation for $\tau = \sigma_{ny}/\mu$:

$$\frac{\tau_{[j,k]}^{m+1/2} - \tau_{[j,k]}^{m-1/2}}{\Delta t} = \frac{v_k^m - v_j^m}{d_{[j,k]}}. \tag{7}$$

Here, $d_{[j,k]}$ is the distance between the Delaunay vertices k and j. Note that the velocity is updated at time steps $m, m+1, m+2, \ldots$ while the stress is updated at time steps $m+1/2, m+3/2, \ldots$

In Eqs. (6) and (7) we have made use of the fact that $d_{[j,k]}$ is perpendicular to $l_{[j,k]}$ which is guaranteed by the properties of the Delaunay and Dirichlet tessellations described above. This means that Eq. (7) always computes the stress normal to the line element $l_{[j,k]}$. In other words, stress is always computed in the local coordinate system of Figure 1.

Since in Eq. (6) v_j^m is assumed to be constant within the Voronoi cell, we can rewrite this equation as

$$v_j^m = v_j^{m-1} + \left(\frac{\Delta t}{\sum_{k=1}^{N_k} A_{[j,k]}\rho_{[j,k]}}\right)\sum_{k=1}^{N_k} l_{[j,k]}\mu_{[j,k]}\tau_{[j,k]}^{m-1/2}. \tag{8}$$

The quantities $\Delta t/(\sum_{k=1}^{N_k} A_{[j,k]}\rho_{[j,k]})$ and $l_{[j,k]}\mu_{[j,k]}$ can be precomputed for every grid point. Note that each term $l_{[j,k]}\mu_{[j,k]}$ involves two Delaunay cells and thus two values of μ. Each term is therefore of the form

$$l_1\mu_1 + l_2\mu_2$$

where l_1 and l_2 ($l_1 + l_2 = l_{[j,k]}$) are the parts of $l_{[j,k]}$ in the first and the second two Delaunay cell, respectively, and μ_1 and μ_2 are the values of μ in the two Delaunay cells.

We rewrite Eq. (7) as

$$\tau_{[j,k]}^{m+1/2} = \tau_{[j,k]}^{m-1/2} + \Delta t\frac{v_k^m - v_j^m}{d_{[j,k]}}. \tag{9}$$

Equations (8) and (9) are our final equations for updating the velocity and stress, respectively.

It is interesting to note that the method can be formulated in an analogous way for rectangular rather than triangular Delaunay elements. In this case uniform grid spacing will lead to the usual FD equations for staggered grids.

P-SV WAVES IN 2-D

The P-SV case can be derived analogously to the SH-case. We define the particle velocities in a Cartesian coordinate system $\{\hat{x}, \hat{y}\}$ while we define the stress at each point in a local coordinate system $\{\hat{n}, \hat{s}\}$. Analogously to Eqs. (2) and (3) we then obtain

$$\begin{aligned} \iint_A dA\, \rho \frac{\partial v_x}{\partial t} &= \oint_{\partial A} ds\, (\sigma_{nn} \cos\phi - \sigma_{nt} \sin\phi) \\ \iint_A dA\, \rho \frac{\partial v_z}{\partial t} &= \oint_{\partial A} ds\, (\sigma_{nn} \sin\phi + \sigma_{nt} \cos\phi) \end{aligned} \tag{10}$$

$$\begin{aligned} \frac{\partial \sigma_{nn}}{\partial t} &= (\lambda + 2\mu)(\frac{\partial v_x}{\partial n} \cos\phi + \frac{\partial v_z}{\partial n} \sin\phi) \\ \frac{\partial \sigma_{nt}}{\partial t} &= \mu(-\frac{\partial v_x}{\partial n} \sin\phi + \frac{\partial v_z}{\partial n} \cos\phi). \end{aligned} \tag{11}$$

In Eqs. (10) and (11), ϕ is defined as the angle between the x-axis and the direction $\hat{n}$, measured counterclockwise from x.

The discrete formulation of Eq. (10) becomes [analogously to Eq. (8)]:

$$v_{xj}^m = v_{xj}^{m-1} + \left(\frac{\Delta t}{\sum_{k=1}^{N_k} A_{[j,k]} \rho_{[j,k]}} \right) \sum_{k=1}^{N_k} l_{[j,k]} [(\lambda_{[j,k]} + 2\mu_{[j,k]}) \eta_{[j,k]}^{m-1/2} \cos\phi - \mu_{[j,k]} \xi_{[j,k]}^{m-1/2} \sin\phi]$$

$$v_{zj}^m = v_{zj}^{m-1} + \left(\frac{\Delta t}{\sum_{k=1}^{N_k} A_{[j,k]} \rho_{[j,k]}} \right) \sum_{k=1}^{N_k} l_{[j,k]} [(\lambda_{[j,k]} + 2\mu_{[j,k]}) \eta_{[j,k]}^{m-1/2} \sin\phi + \mu_{[j,k]} \xi_{[j,k]}^{m-1/2} \cos\phi] \tag{12}$$

Here, $\eta = \sigma_{nn}/(\lambda + 2\mu)$ and $\xi = \sigma_{nt}/\mu$. The quantities

$$\Delta t / \sum_{k=1}^{N_k} A_{[j,k]} \rho_{[j,k]},$$

$$l_{[j,k]}(\lambda_{[j,k]} + 2\mu_{[j,k]}),$$

$$l_{[j,k]} \mu_{[j,k]},$$

$$\cos\phi,$$

$$\sin\phi$$

can be precomputed for each grid point.

The discrete formulation of Eqs. (11) becomes [analogously to Eq. (9)]:

$$\begin{aligned} \eta_{[j,k]}^{m+1/2} &= \eta_{[j,k]}^{m-1/2} + \frac{\Delta t}{d_{[j,k]}} [(v_{xk}^m - v_{xj}^m) \cos\phi + (v_{zk}^m - v_{zj}^m) \sin\phi] \\ \xi_{[j,k]}^{m+1/2} &= \xi_{[j,k]}^{m-1/2} + \frac{\Delta t}{d_{[j,k]}} [-(v_{xk}^m - v_{xj}^m) \sin\phi + (v_{zk}^m - v_{zj}^m) \cos\phi]. \end{aligned} \tag{13}$$

BOUNDARY CONDITIONS

The free-surface boundary condition can be easily satisfied by Eqs. (8) and (12). These equations can be directly applied to updating the particle velocity on the free surface. The condition there is that the stress vanishes. Therefore, instead of summing the stress over a closed curve in Eqs. (8) and (12), as in the interior of the region, the stress is summed over an open curve at the free surface. This is illustrated in Figure 4, which shows examples of these curves for both a point on the surface and a point in the interior. Both curves are shown as thick lines.

At all other boundaries we implement absorbing boundary conditions. This is done in a similar way to standard FD schemes. We use Higdon's (1986, 1987) boundary condition which is of the form

$$\prod_{j=1}^{p}(\cos\theta_i\frac{\partial}{\partial t}-\alpha\frac{\partial}{\partial x_k})v=0 \tag{14}$$

where θ_i is the incident angle of maximum absorption, α is the wave speed and x_k is $+x/-x/+z$ for the right/left/bottom boundary. Here we will only discuss the implementation of a first-order ($p=1$) boundary condition. However, a higher order boundary condition can be applied in an analogous way.

In order to implement the boundary condition more easily, we use a Delaunay mesh whose elements at the left, right, and bottom boundaries are as shown in Figure 5a. In this mesh the elements at the bottom are equilateral triangles while the elements at the left and right boundaries are right triangles. For points on the left and right boundaries, the derivative of the velocity with respect to x is needed. Figure 5 a shows the points used to approximate this derivative at a point k on the right boundary. The derivative is computed as

$$\frac{\partial v}{\partial x}\approx\frac{v_k-v_j}{d_{[j,k]}}. \tag{15}$$

At the bottom we need the derivative with respect to z. Figure 5b shows a point P on the lower boundary. The unit vectors $\hat{n}^1$ and $\hat{n}^2$ point in the directions away from the two neighboring points above P. The derivative of v in the z-direction at P can be expressed in terms of the derivatives in these directions as

$$\frac{\partial v}{\partial z}=\frac{n_x^2(\partial v/\partial n^1)-n_x^1(\partial v/\partial n^2)}{n_z^1n_x^2-n_z^2n_x^1}. \tag{16}$$

For the geometry of Figure 5, we obtain $n_z^1=n_z^1=\cos 30^\circ=\sqrt{3}/2$ and $-n_x^1=n_x^2=\sin 30^\circ$. Equation (16) then becomes

$$\frac{\partial v}{\partial z}=\frac{1}{\sqrt{3}}(\frac{\partial v}{\partial n^1}+\frac{\partial v}{\partial n^2}). \tag{17}$$

The boundary conditions are only applied to the particle velocity. The stress is updated as before [Eqs. (9) and (13)].

A NUMERICAL EXAMPLE

We demonstrate the technique with a simple example of SH-wave propagation. We use a grid that consists of two parts. The spacing is 6 m in the bottom and 3 m in the top part. Each of these subgrids is uniform; i.e., the Delaunay elements are equilateral triangles everywhere except at the left and right boundaries and at the transition between the two subgrids.

The purpose of this example is to show that there are no numerical artifacts associated with the transition between the two subgrids, i.e., that grid irregularity causes no numerical problems. This is most easily shown by modeling wave propagation in a homogeneous medium. In this example, the wave speed is 1700 m/s everywhere in the model. We use an impulsive source excitation as proposed by Alford *et al.* (1974) and Virieux (1984) with a dominant frequency of 16.7 Hz. Thus, there are 17 points per wavelength in the bottom part of the grid, and 34 in the top part.

Figures 6a–f show a series of snapshots of the particle velocity at 9.6 ms time intervals. Also shown is the Delaunay grid on which the velocity is defined. The figures show an SH-wave propagating away from the source. In Figure 6c the wave front has reached the free surface at the top and is reflected back into the medium. In Figures 6d–f two downward propagating waves can be observed—the direct wave and the reflection from the free surface.

The wavefront can be seen to cross the transition between the two subgrids without causing any reflections or distortions. This demonstrates that our method can handle the grid irregularities in this area without problems.

DISCUSSION AND CONCLUSIONS

The method described here is generally of first-order accuracy in space. However, if the grid is uniform, the difference operators of Eqs. (8), (9), (12), and (13) become exactly centered and the accuracy becomes second-order. Thus in the example of Figure 6 the accuracy is second order everywhere except at the transition between the two subgrids. Generally, one would parameterize a model in a similar way as we have done in Figure 6, i.e., using uniform grids in regions where the elastic parameters are constant and change the grid spacing only at transitions between different regions in order to accommodate changes in medium parameters and in order to force grid points to lie on interfaces. Then, in most regions of the model the accuracy will be second-order in space.

Our method can be extended to 3-D because the concepts of Delaunay and Dirichlet tessellations exist in 3-D as well. The Delaunay cell in 3-D is a tetrahedron and the Voronoi cell is a polyhedron. In 3-D, integrations over areas become integrations over volumes, and integrations over curves become integrations over areas. These integrations can be approximated by summations analogous to the 2-D case.

As we have demonstrated, the FV method is an attractive alternative to FD that allows the model to be parameterized on an irregular grid. This should potentially lead

to more accurate results than FD. Also, the greater flexibility in parameterizing the model should make FV computationally more efficient than FD. There are, however, two points to be considered. First, our method like any method that uses irregular grids requires computer memory to store the grid geometry. The total memory requirement is thus higher than for traditional FD methods. Second, the computation of the grid itself requires a certain amount of time. Computing a grid for our scheme involves several steps: (1) the locations of the Delaunay vertices are defined; and (2) then the Delaunay and Dirichlet meshes are computed; and (3) the medium properties are assigned to the Delaunay elements. To obtain an efficient model parameterization by performing these steps is not a trivial task, and further research is needed in this area. In any case, computing the grid will take some computation time in addition to the actual modeling.

We plan to address these points in a future study on the comparison of our method with FD in terms of both accuracy and computational efficiency. Since our results look very promising so far, we believe that we will find our method to be superior to FD in many cases.

ACKNOWLEDGMENTS

I thank Rick Gibson for critically reading this manuscript. This work was supported by the Air Force Technical Applications Center/Phillips Laboratory under Contract No. F19628-95-C-0091. Additional funding was provided by the Reservoir Delineation Consortium of the Earth Resources Laboratory, MIT.

REFERENCES

Alford, R.M., Kelly, K.R., and Boore, D.M., 1974, Accuracy of finite-difference modeling of the acoustic wave equation, *Geophysics, 39*, 834–842.

Dirichlet, G.L., 1850, Über die Reduktion der positiven quadratischen Formen mit drei unbestimmten ganzen Zahlen, *J. Reine u. Angew. Math., 40*, 209–227.

Delaunay, B.N., 1934, Sur la sphere vide, *Bull. Acad. Science, USSR VII: Class. Sci. Math.*, 793–800.

Dormy, E. and Tarantola, A., 1995, Numerical simulation of elastic wave propagation using a finite-volume method, *J. Geophys. Res., 100*, 2123–2133.

Higdon, R.L., 1986, Absorbing boundary conditions for difference approximations to the multi-dimensional wave equation, *Math. Comp., 47*, 437–459.

Higdon, R.L., 1987, Numerical absorbing boundary conditions for the wave equation, *Math. Comp., 49*, 65–90.

Lee, C.F.,McCartin, B.J., Shin, R.T., and Kong, J.A., 1994, A triangular-grid finite-difference time-domain method for electromagnetic scattering problems, *Journal of Electromagnetic Waves and Applications, 8*, 449–470.

Miller, J.H. and Wang, S., 1994, An exponentially fitted finite volume method for the numerical solution of 2D unsteady incompressible flow problems, *J. Comp. Phys., 115*, 56–64.

Virieux, J., 1984, SH-wave propagation in heterogeneous media: velocity-stress finite-difference method, *Geophysics, 49*, 1933–1957.

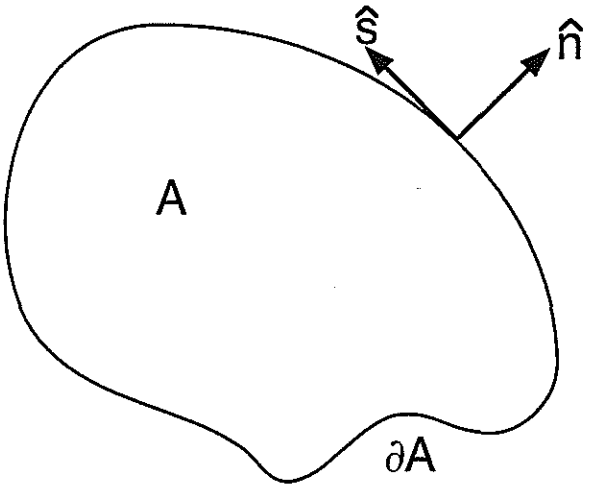

Figure 1: Local coordinate system used to define the stress.

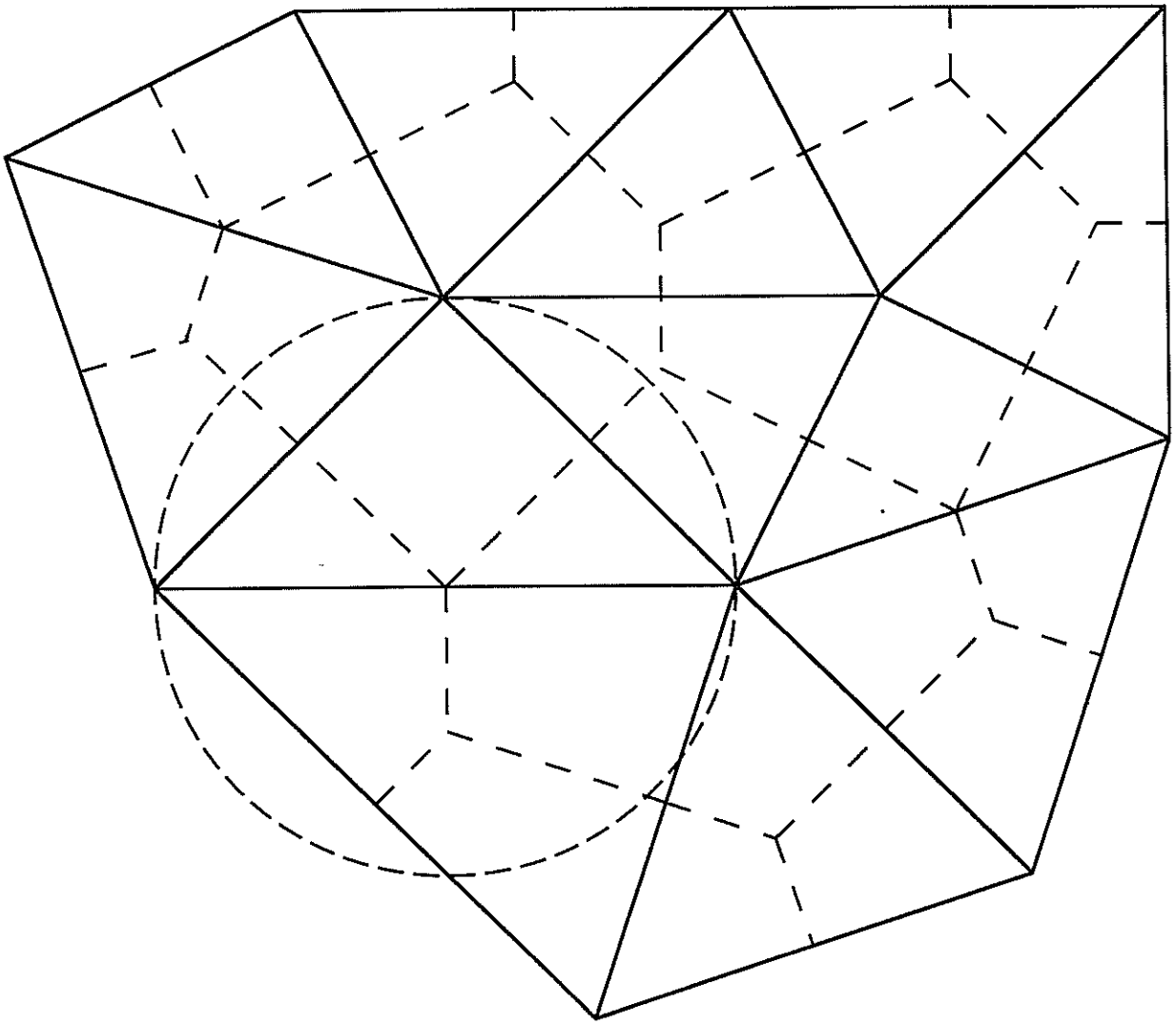

Figure 2: Delaunay mesh (solid) and Dirichlet tessellation (dashed). Also shown is a circumcircle of a Delaunay element having a vertex of a Voronoi polygon as its center.

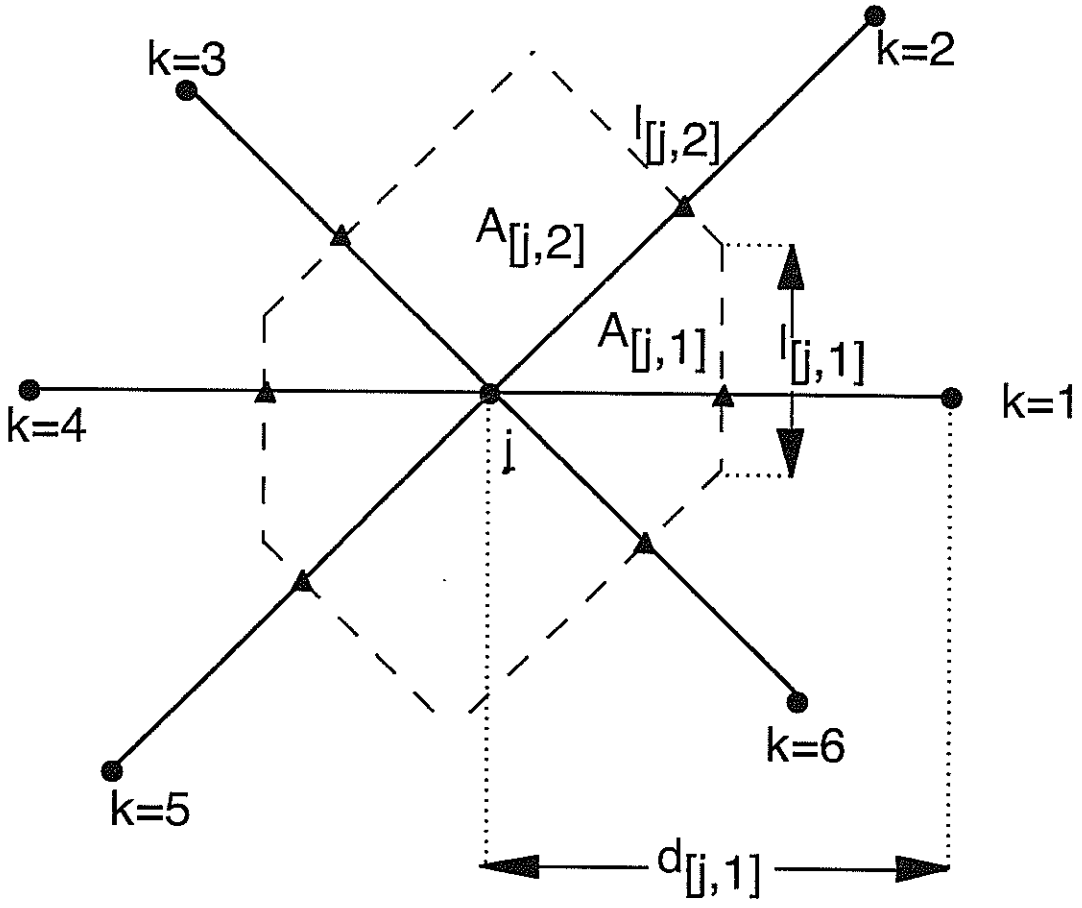

Figure 3: Indexing used for the computations. The particle velocities are defined at the Delaunay vertices (circles) and the stresses at the points marked by triangles. In order to update particle velocities the stresses are summed over the corresponding Voronoi polygons.

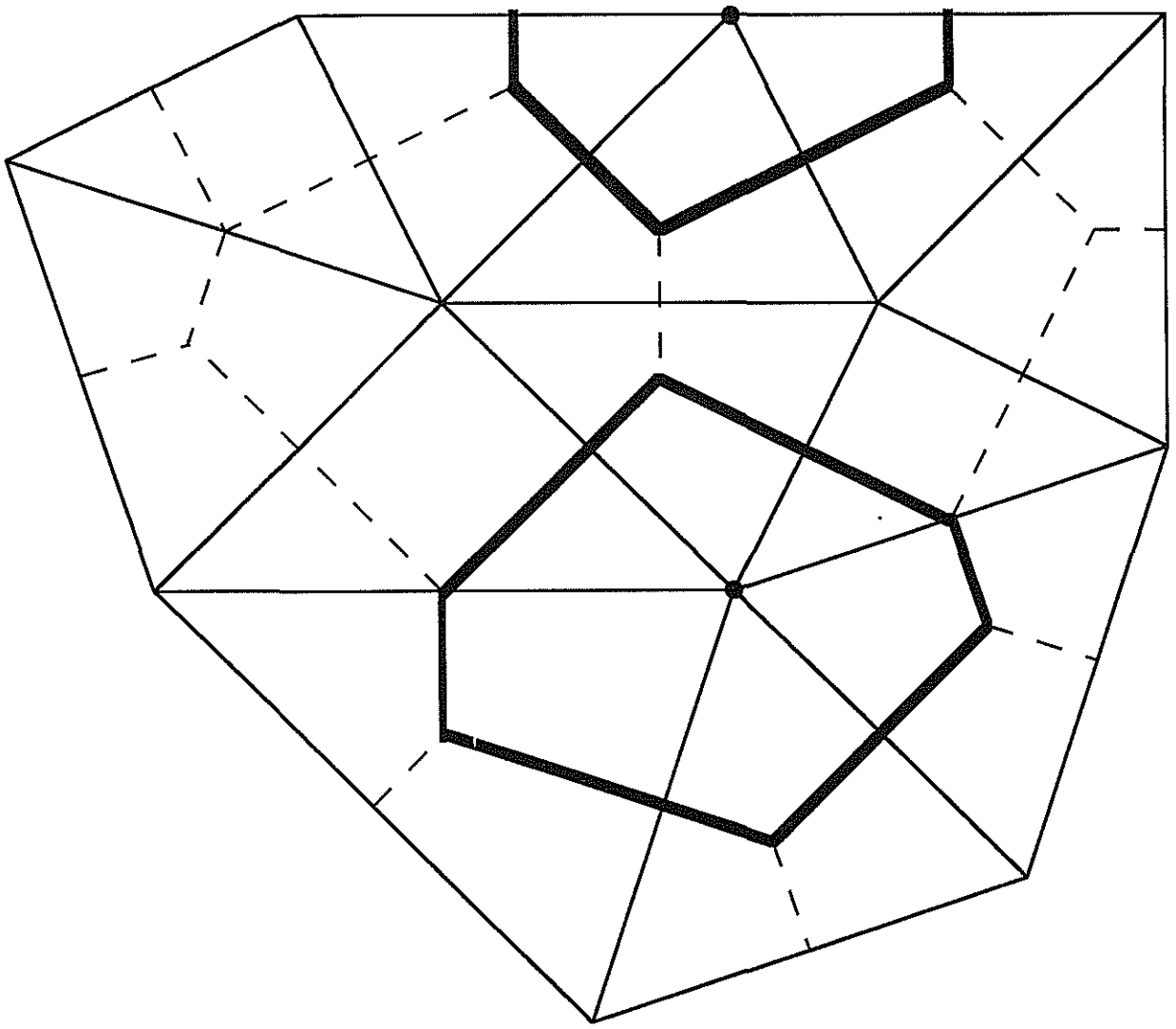

Figure 4: Examples of Voronoi polygons over which the stress is summed in order to update the particle velocity. Two polygons are shown as thick lines, and the corresponding velocity points as circles. One of these polygons is for a point on the free surface and is open, whereas the other is for a point in the interior and is closed.

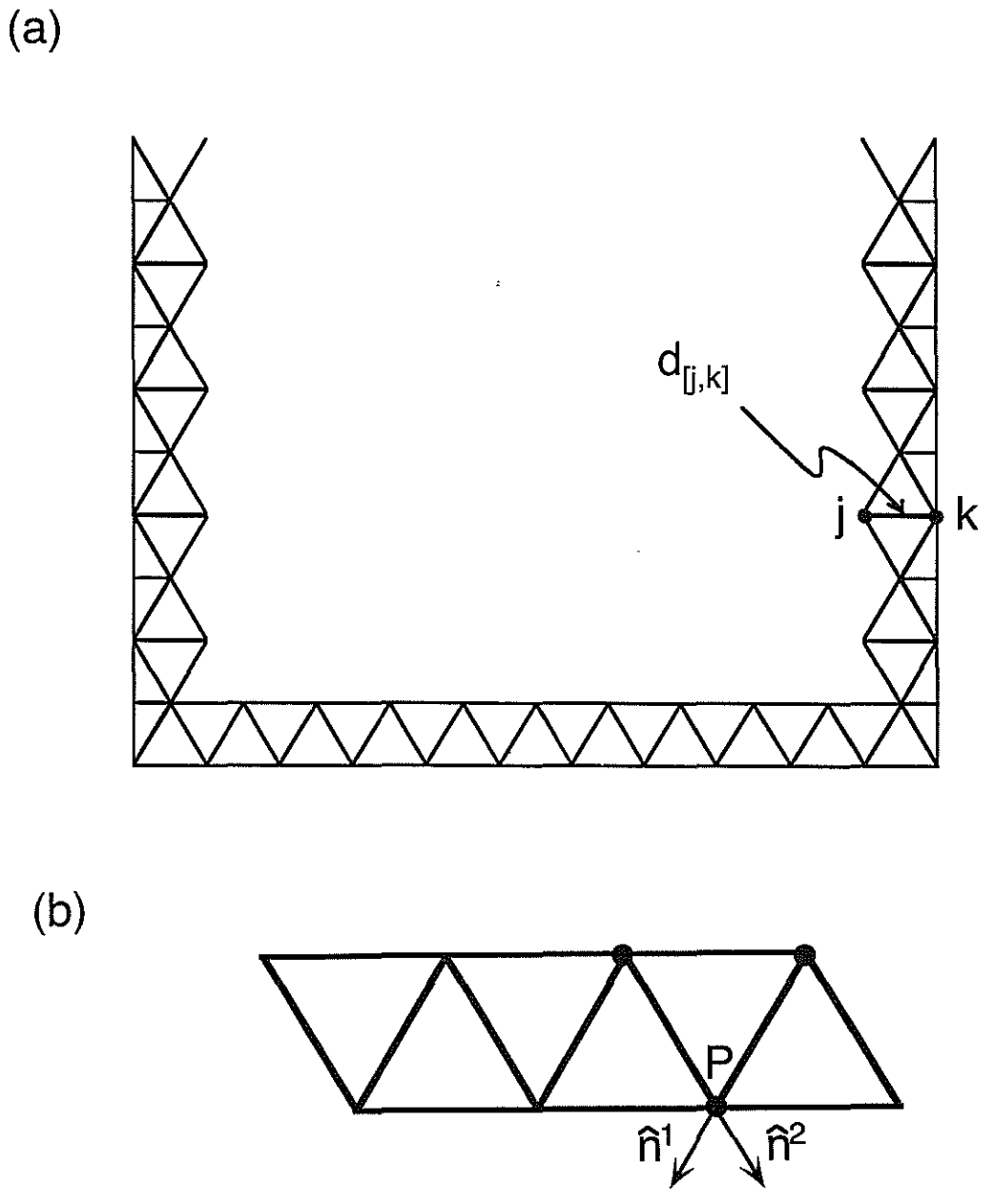

Figure 5: (a) Grid geometry used at the left, right, and bottom boundaries for the implementation of the absorbing boundary condition; (b) definition of directions $\hat{n}^1$ and $\hat{n}^2$ at the bottom boundary (see main text).

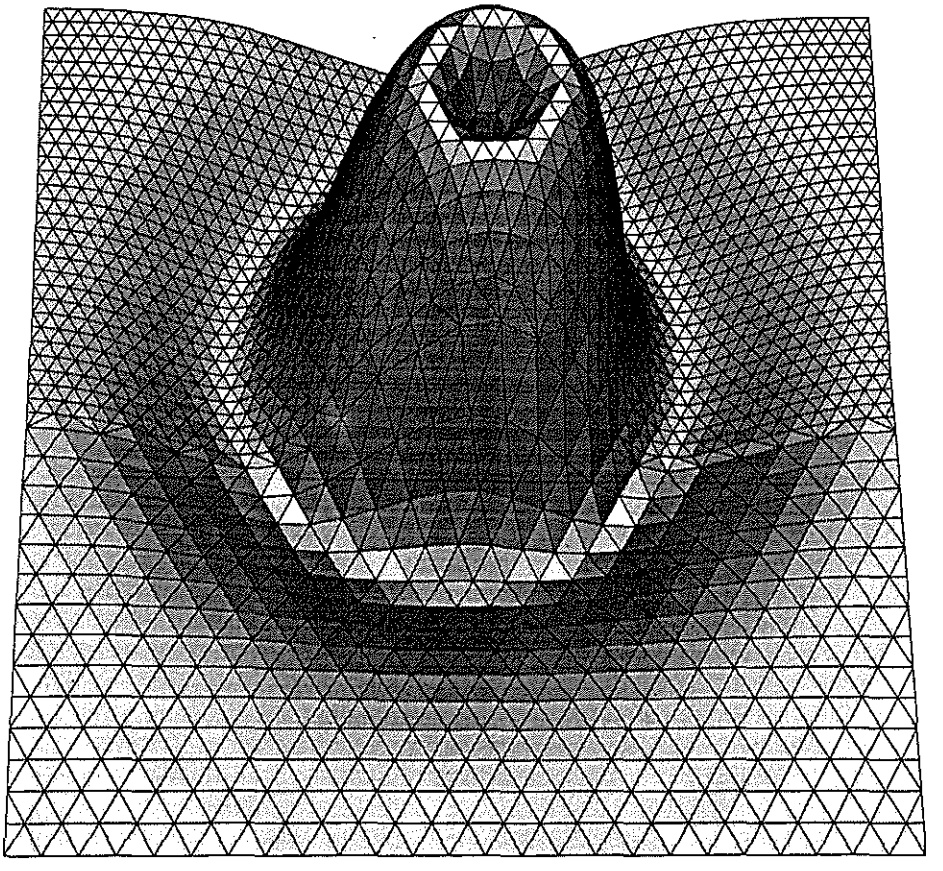

Figure 6a: Snapshot of the particle velocity at different time steps. The time difference between successive snapshots is 9.6 ms. The series of snapshots show the propagation of an SH wave. The Delaunay mesh on which the particle velocity is defined is also shown.

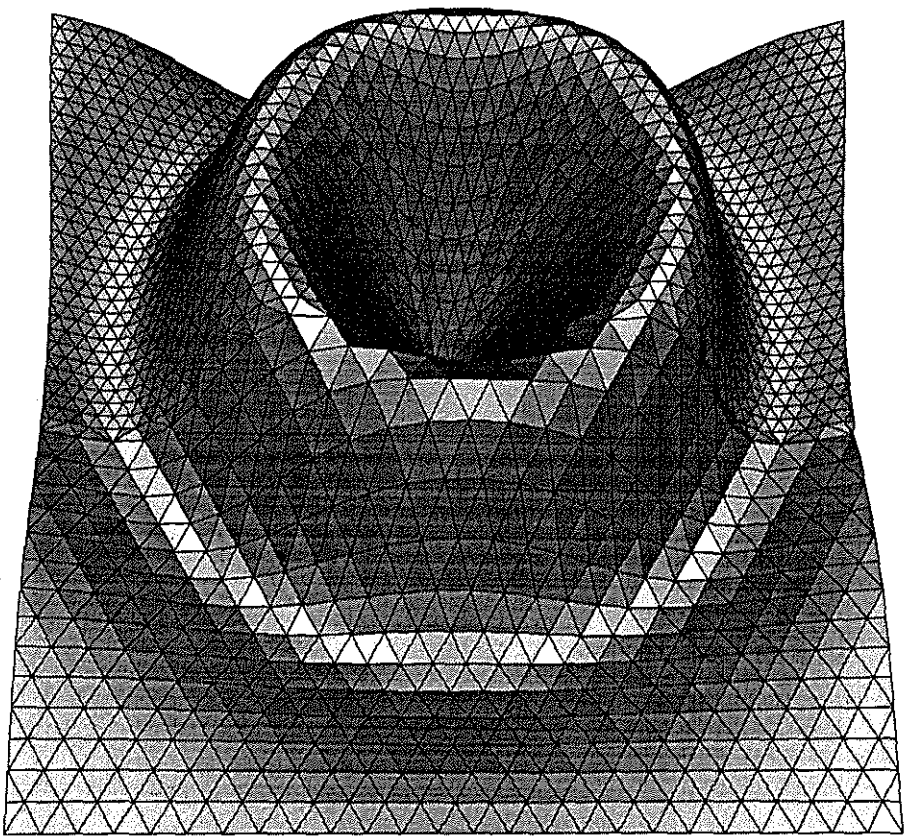

Figure 6b.:

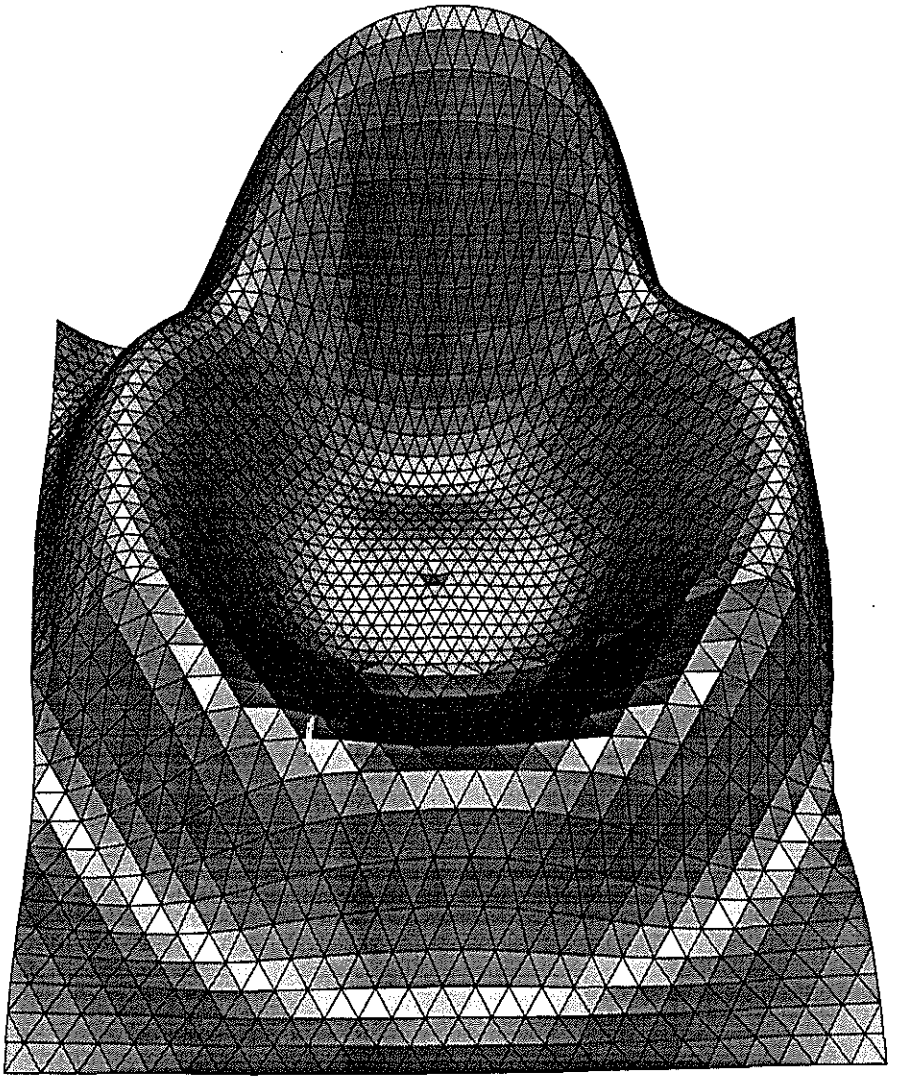

Figure 6c:

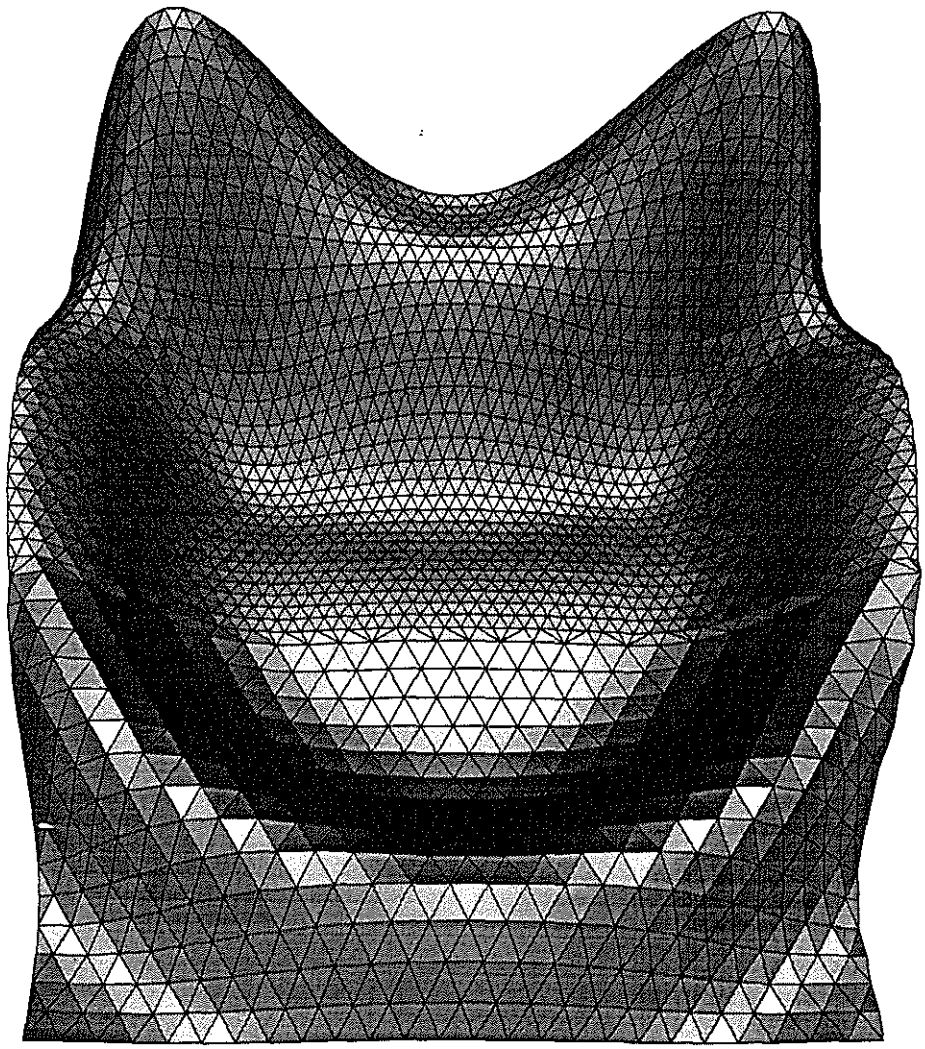

Figure 6d:

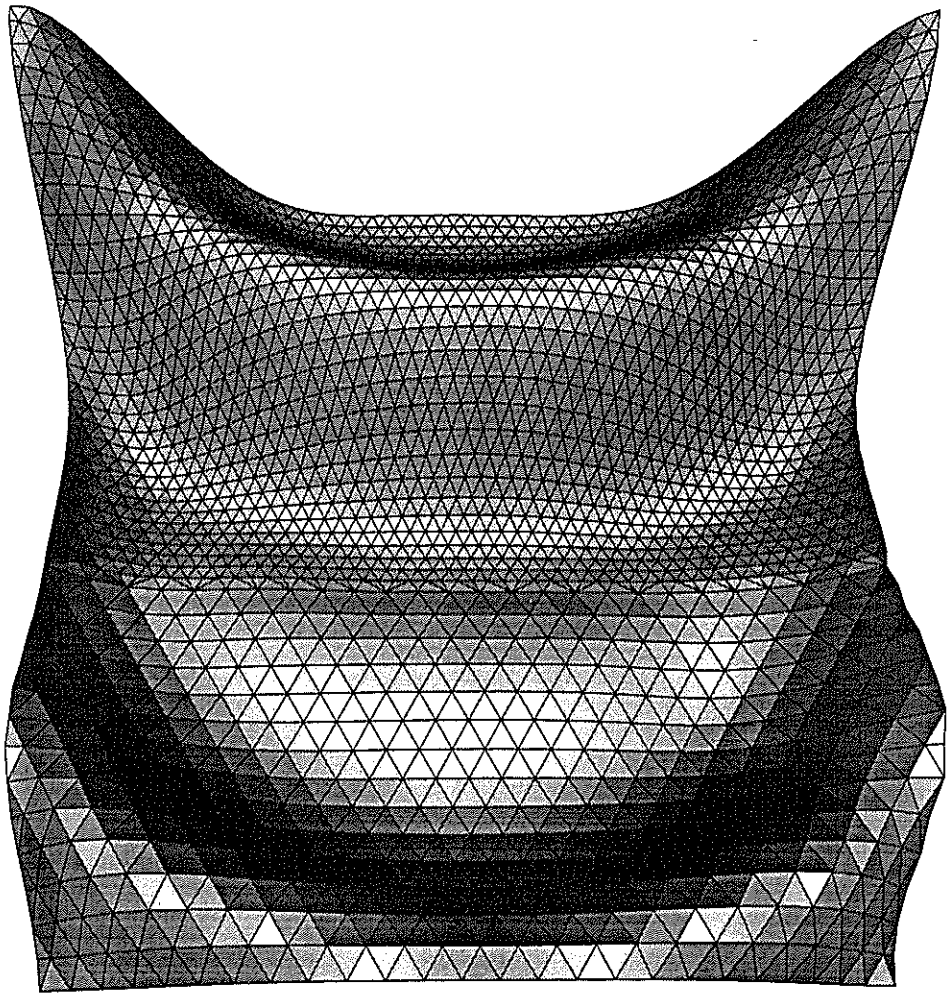

Figure 6e:

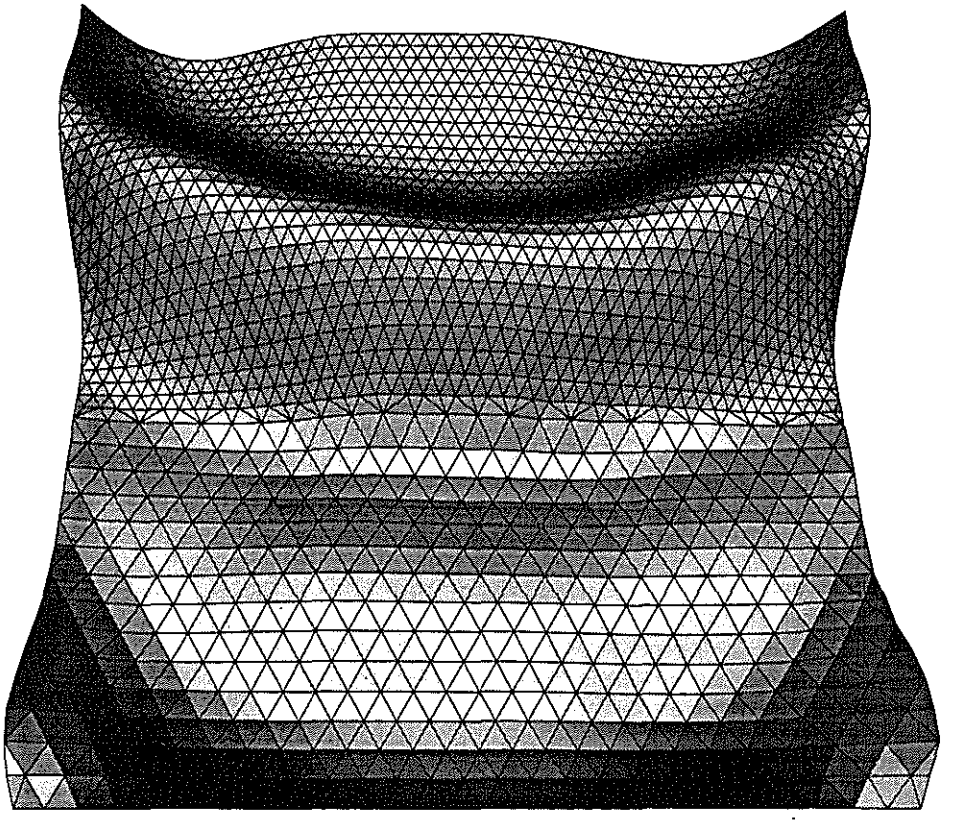

Figure 6f: